Desalination and Water Treatment
www.deswater.com

doi: 10.5004/dwt.2020.26103

201 (2020) 204–218
October

Evaluation of promising coagulant shrimp shell on paint factory effluent: studies on mixing pattern, isotherms, kinetics, and thickener design

Vishali Solaiappan*, Rajdeep Mukherjee, Picasso Sengupta, Nihal Rao

Department of Chemical Engineering, SRM Institute of Science and Technology, Chennai 603 203, Tamil Nadu, India, Tel. +91-94438 83562; email: meet.vishali@gmail.com (V. Solaiappan), Tel. +91-98316 85593; email: rjdp0494@gmail.com (R. Mukherjee), Tel. +91-97104 30335; email: picassosengupta@gmail.com (P. Sengupta), Tel. +91-97909 61478; email: nihal1050@gmail.com (N. Rao)

Received 13 November 2019; 6 May 2020

ABSTRACT

Lab-scale experiments were carried out to examine the effect of rapid mixing rate, slow mixing rate, settling span, velocity gradient, and Camp number to study the color and turbidity removal from simulated paint factory effluent (SPFE) using shrimp shell powder and chitosan as a coagulant. At the isothermal conditions the optimized results were found as 200 rpm of rapid mixing for 5 min, 80 rpm of slow mixing for 20 and 40 min settling span with velocity gradient of 562 1/s and Camp number 8.05. An equilibrium two-parameter and three-parameter isotherm models were tried for the obtained optimum parameters along with error functions. The results have confirmed the suitability of the selected coagulant toward the removal of pollutants. To interpret the rate of transport of pollutants in the direction of coagulant, kinetic studies were executed and identified that the treatment process was following second-order kinetic model. The thickener area required for the 1,000 L/d flow of SPFE was calculated using Kynch theory, which was in the increasing trend while boosting the initial concentration of SPFE.

Keywords: Paint factory effluent; Shrimp shell; Coagulation; Isotherm model; Kinetics

1. Introduction

All water including industrial wastewater contains both suspended and dissolved particles. Water threat forced the researchers to find a better solution to convert the wastewater into usable forms of water. Among the wastewaters from different industrial resources, the paint industry also contributes major pollutants like color, biochemical oxygen demand (BOD), chemical oxygen demand (COD), turbidity, heavy metals, oil and grease, and so on. Paint industry effluent has been treated using many techniques so far. But based on the literature review, the coagulation process exhibits its positivity in the reduction of pollutant in a higher level [1].

Nowadays coagulation and flocculation get more attention in the separation of the suspended solid portion from the effluent. The settling property of the suspended particle may vary based on the particle origin, particle shape, size, density, and charge. The coagulation process combines three steps in it viz., (i) coagulation (addition of coagulant with the effluent), (ii) flocculation and sedimentation (flocs formation), and (iii) sedimentation (floc settling). The predominant mechanism behind the coagulation is charge neutralization [2].

For all raw water types, several water quality parameters affect coagulation performance, including the amount of particulate material, natural organic matter properties (such as size, functionality, charge, and hydrophobicity),

* Corresponding author.

coagulant type, dose, mixing conditions, pH, and temperature [3]. By enhancing the performance of the coagulation process, the performance of the forthcoming unit operations viz., sand filtration, membrane operations might be favored. The settling span of the flocs can be lessened by boosting the magnitude and density of the particle [4].

Good coagulation is achieved by a high-energy, rapid-mixing to properly disperse the coagulant into the wastewater and enhance the collision of particles. Over-mixing does not influence on coagulation step but disturbs the flocculation step by the re-dispersion of flocs. But insufficient mixing and contact time will affect the coagulation step [5]. The coagulation and flocculation process has to make the denser and larger flocs to enhance the settling process [6].

In the flocculation step, high molecular weight compounds named coagulant aids may be added to promote the floc strength and to add weight so that the settling rate will be increased. The floc is ready for the sedimentation process once the optimum size and strength are reached [7].

Generally, either a gravity settling or sedimentation is a choice for the solid–liquid separation. Both processes are simpler in nature. The interaction between the liquid and solid phases converts the process into more complex to understand [8]. The settlement characteristics of the suspended particles differ with its size. Stoke's Law helps to estimate the terminal settling velocity of the larger size particle, whereas fine particles are affected majorly by charge, concentration, size, shape, and so on. The adsorption between the coagulant and the effluent reduces the surface potential of particles. As a consequence, the adhesive sediment particles form flocs [9].

Fenneropenaeus indicus (shrimp) shell waste was generated in the vast mass globally. Most of the wastes were disposed of by ocean dumping. Chitosan, a cationic polymer derived from the shells of crab, shrimp is the abundant bio polymer. This made the shrimp shell waste as an active coagulant and adsorbent. Oily produced wastewater was successfully treated using the chitosan coagulant obtained from shrimp shells [10]. Shrimp shells were used as an adsorbent in the removal of arsenic from groundwater [11] and in the removal of direct dyes from wastewater [12].

The current work focused to study the settling behavior of the flocs formed during the coagulation process of paint industry wastewater. Here, the settling velocity of an aggregate suspension in a settling tube and the solid volume concentration was measured [13]. Through color and turbidity removal the treatment efficiency was measured. The experimental values were supported by the isotherm and kinetic studies. The required thickener area was calculated using the Kynch theory for 1,000 L/d flow rate. The flow sheet of the current study is consolidated in Fig. 1.

2. Materials and methods

2.1. Materials

Throughout the experiments, analytical grade (AR) chemicals bought from Merck, India were used. With the help of the commercially white primer and an acrylic-based blue colorant (5% (v/v)), the simulated water-based paint factory effluent (SPFE) was prepared. Different samples with varying initial concentrations viz., 1,200; 1,350; 1,850; 2,200; and 2,700 mg/L were prepared and numbered as sample numbers 1–5, respectively. The real water-based paint factory effluent (RPFE) was collected from a paint factory located in Chennai, South India. The physical–chemical properties of both the effluents were listed in Table 1. Standard Methods were followed for the determination of characterization [14].

The *F. indicus* (Indian shrimp) shells were acquired from the local sea food market located in Chennai, South India. The shrimp shells were washed, sun-dried for 24 h, powdered (SSP) with a kitchen mixer, and sieved through a 0.5 mm sieve. Chitosan is a linear cationic polymer of high molecular weight commonly derived from chitin, obtained from the outer shells of shrimps was used as a conventional chemical coagulant. It was purchased as flakes and powdered, sieved to 0.5 mm size.

The *F. indicus* (Indian shrimp) shells were acquired from the local seafood market located in Chennai, South India. The shrimp shells were washed, sun-dried for 24 h, powdered (SSP) with a kitchen mixer and sieved through a 0.5 mm sieve. Chitosan is a linear cationic polymer of high molecular weight commonly derived from chitin, obtained from the outer shells of shrimps was used as a conventional chemical coagulant. It was purchased as flakes and powdered, sieved to 0.5 mm size.

2.2. Methods

To treat a liter of SPFE (1,200 mg/L), 400 mL of shrimp shell eluate prepared using 3N NaCl and 40 g of shrimp shell was used. Similarly, 600 mL of chitosan extract prepared using 5 g of chitosan powder and 0.1N of HCl was used. The preparation of coagulation extract and optimized results were discussed in previous study [15].

The experiments were performed using jar test apparatus (Deep Vision-India) comprised of six spindles and a speed range of 50–300 rpm with an illuminated base for measuring the flocs. It was then regulated to rapid mixing for 5 min at 50–300 rpm, followed by slow mixing for 20 min at 20–100 rpm and settling period of 5–60 min. A sample of the supernatant liquid was taken at regular intervals during the settling period and centrifuged at 10,000 rpm for 5 min. The clarified liquid was used for the measurement of residual color and turbidity. The amount of sludge obtained was also noted. The above process was recast to optimize the operating variables viz., rapid mixing rate, low mixing rate, settling span, velocity gradient, and Camp number. All the experiments were repeated at least thrice for concordance and the mean values were taken for a plot.

2.3. Physico-chemical analysis

The coagulation process was evaluated in terms of the removal of color and turbidity. All the parameters mentioned in Table 1 were measured using standard procedures [14]. The color was measured using an SL218 double UV visible spectrophotometer (Elico – India) at λ_{max} 612 nm for SPFE and 252 nm for RPFE. Turbidity was measured using digital nephelo-turbidity meter 132 (Elico – India) and expressed in nephelometric turbidity units (NTU). pH was adjusted using a digital pH meter MK. V.I (Elico – India).

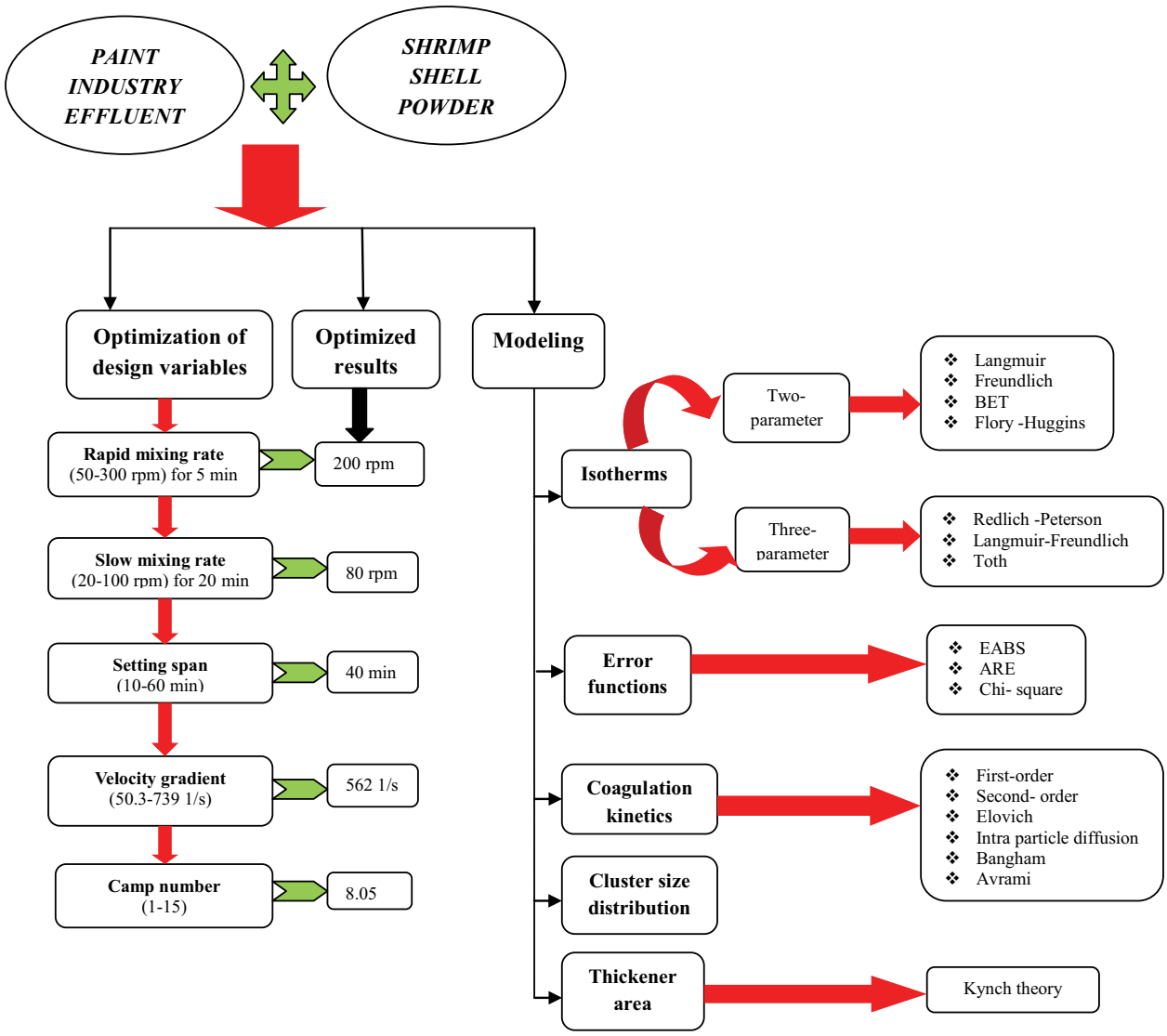

Fig. 1. Flow sheet of the current study.

Table 1
Physico-chemical characteristics paint factory effluent

Concentration (except for pH, color and turbidity, and viscosity)		
Parameters	Simulated paint factory effluent (SPFE) sample no. 5	Real paint factory effluent (RPFE)
pH at 25°C	8.4–8.6	7.03
Color	Blue	Dark black
Total dissolved solids, mg/L	214	1,234
Total suspended solids, mg/L	11,286	300
Oil and grease, mg/L	19	15
Sulfate as SO_4, mg/L	24	115
Chemical oxygen demand (COD), mg/L	2,700	1,760
Biochemical oxygen demand, mg/L (3 d incubated at 27°C)	1,254	880
Turbidity, NTU	5,210	198.5
Viscosity, kg/m s	0.0144	0.015

3. Results and discussion

3.1. Coagulation using shrimp shell coagulant

3.1.1. Effect of rapid mixing rate on removal efficiency

To evaluate the rapid mixing rate in the coagulation process, it was varied between 50 and 300 rpm for 5 min. The importance of the rapid mixing rate is to ensure the proper mixing of coagulant with the effluent so that the removal efficiency will be enhanced. The removal efficiency was in the increasing trend when the mixing rate was raised, but beyond 200 rpm, there was no appreciable change in the removal efficiency. So 200 rpm was concluded as the optimized rapid mixing rate for treatment using SSP, and the observed efficiencies (Fig. 2) were 93% (for color) and 82% (for turbidity) [16].

3.1.2. Effect of slow mixing rate on removal efficiency

The significance of selecting the optimum slow mixing rate is to confirm the formation of proper flocs during the flocculation after the rapid mixing period. The treatment was performed at the rapid mixing rate of 200 rpm for 5 min, followed by a slow mixing span of about 20 min, and the rate was ranged between 20 and 100 rpm. From Fig. 3, it was noticed that the removal efficiency was improved when the slow mixing rate was increased till 80 rpm, which ensures that the better floc formation to facilitate the settling. The values were (Color) 92%, (Turbidity) 83%. The reason for the decreasing trend beyond 80 rpm was that the over mixing might break the floc formation and encourages the re-dispersion [17].

3.1.3. Effect of the setting span on removal efficiency

The color and turbidity removal efficiencies were plotted against the settling span and shown in Fig. 4 and it was increased as the settling time increased (10–60 min). From the results shown, the optimum time identified was 40 min and the removal efficiencies were 88% (color), 74% (turbidity). The believed reason might be due to the movement of the suspended particles in the bulk solution [1].

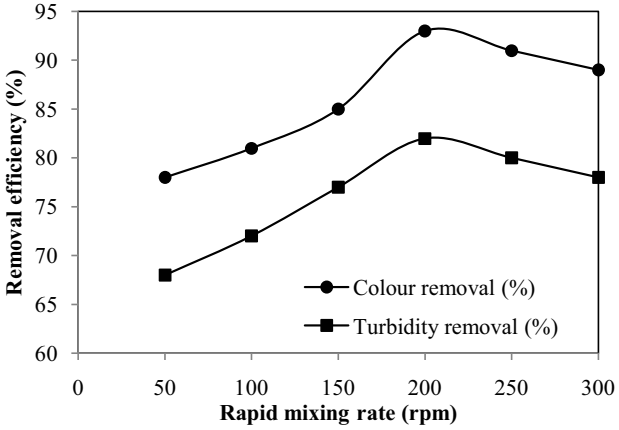

Fig. 2. Effect of rapid mixing rate on removal efficiency.

3.1.4. Effect of velocity gradient on removal efficiency

To govern the chances of the particles colliding together, velocity gradient (G) plays a vital role. The velocity gradient value relies upon power input, effluent dynamic viscosity, and volume of the flocculator. The calculation of the input power was done using the batch mode of jar test experiments using SSP. Fig. 5 shows the effect of the velocity gradient on

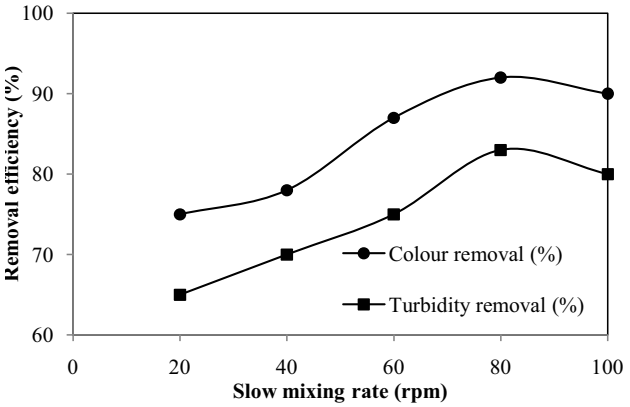

Fig. 3. Effect of slow mixing rate on removal efficiency.

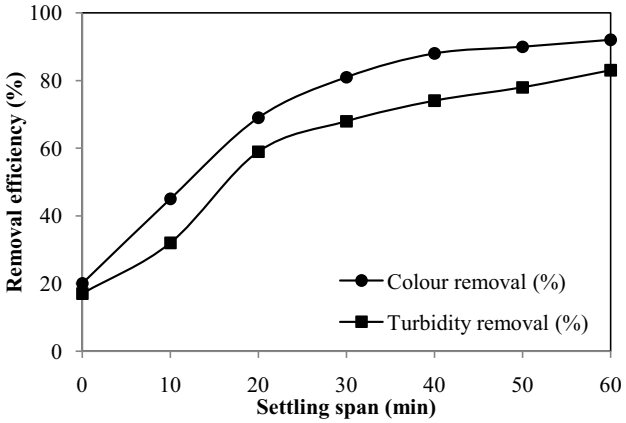

Fig. 4. Effect of the settling span on removal efficiency.

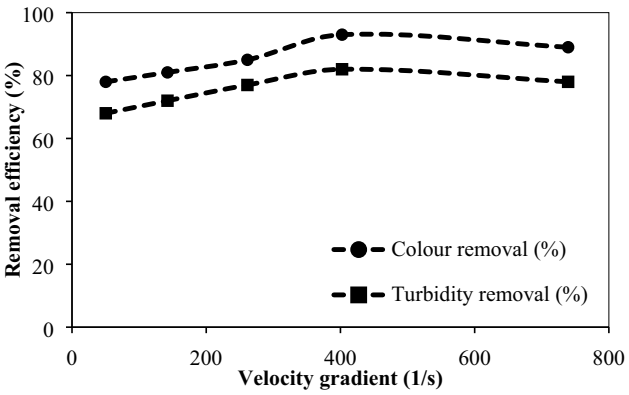

Fig. 5. Effect of velocity gradient on removal efficiency.

the removal efficiency. In these experiments, the coagulation experiments were carried out in the velocity gradient G range of 50.3–739 1/s. The corresponding power input was between 0.073 and 15.741 W. The results (91% color, 80% turbidity) were declared that the velocity gradient (*G*) of 562 1/s and the corresponding mixing rate 250 rpm, input power 9.11 W was in agreement with the better removal efficiency. Floc rupture and floc erosion occurred when excessive-velocity gradient and excessive time was maintained [18].

$$G = \sqrt{\frac{P}{\mu V}} \tag{1}$$

$$P = k_T n^3 D_i^5 \rho \tag{2}$$

where *G* is the average velocity gradient, 1/s; *P* is the input power, W; μ is the effluent dynamic viscosity = 0.0144 Ns/m^2; *V* is the volume of flocculator = 0.002 m^3; k_T is the impeller constant = 35; *n* is the revolution of impeller per second, 1/s; D_i is the impeller diameter = 0.08 m; ρ is the effluent density = 1,098 kg/m^3.

3.1.5. Effect of the Camp number on removal efficiency

The Camp number (Gsf) was obtained by making the product of detention time and velocity gradient [Eq. (3)]. The degree of mixing is based on the power provided, which is measured by the velocity gradient. The effect of the Camp number on the removal efficiency is given in Fig. 6. The removal efficiency was initially boosted up with increasing Camp number and then started decreasing again with a further increase in Camp number. The coagulation process is a combination of coagulation–flocculation–sedimentation. The formation and the growth of the flocs occurred only after the coagulation step bounded. The flocculation step always relies on mixing rate and retention time. The maximum removal of 93% (color) and 82% (turbidity) was noticed at the optimized Camp number of 8.05 [19].

$$G\tau_f = \frac{1}{Q}\sqrt{\frac{PV}{\mu}} \tag{3}$$

where $G\tau_f$ is the Camp number; τ_f is the detention time, s; *Q* is the effluent flow rate = 0.1 m^3/s; *P* is the power requirement, W; μ is the effluent dynamic viscosity = 0.0144 Ns/m^2; *V* is the volume of flocculator = 0.002 m^3.

3.2. Isotherms and error functions

3.2.1. Equilibrium sorption models

The equilibrium of any process is determined by the fitting of the experimental values with the models. These represent the adsorption isotherms. The quantity of adsorbed material required is dependent on the effluent concentration at a constant temperature and the outcome is known as the adsorption isotherm. It indicates an actual approximation of the adsorption capacity and intensity. Models predict the actual quantity of pollutant removal from the effluent at equilibrium by a unit mass of the adsorbent. Their interaction is determined by fitting the experimental values with the models [20].

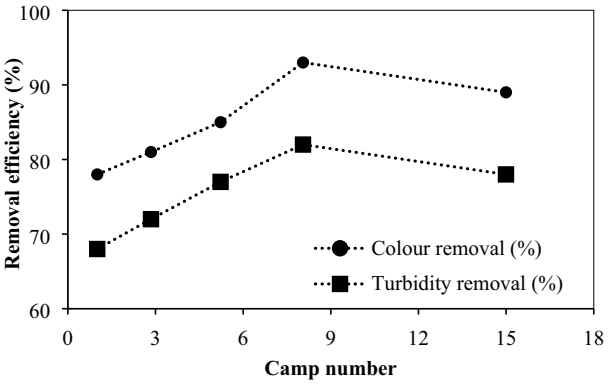

Fig. 6. Effect of Camp number on removal efficiency.

In this study, the data were considered with four two-parameter isotherm models: Freundlich, Langmuir, and Brunauer–Emmett–Teller (BET); three three-parameter models: Redlich–Peterson, Langmuir–Freundlich, and Toth model. All the models mentioned above were solved using non-linear regression analysis in an Excel (solver add-Ins function) spreadsheet since linearization may tamper with the normality of the least-squares. The non-linear form of two-parameter adsorption isotherm models and three-parameter models are tabulated in Tables 2 and 3, respectively.

3.2.2. Error functions

The choicest isotherm model is found only after performing successful error analysis. Error analysis is done with the help of error functions. These error functions represent the net pollutant removal from both the model and the experiment. The best isotherm model is selected based on the least error distribution between the experimental and theoretical values. The smaller the value of the error function, the closer is the replicability of the experimental values with the models [21]. In the present study, three different error functions were studied for error analysis, namely the sum of the absolute errors (EABS), average relative error (ARE), and χ^2 (Chi-square test). Their values were then used for error analysis and to determine the best isotherm fit for the experimental study (Table 4).

3.2.3. Two parameter isotherm model

The evaluated two-parameter isotherm model parameters are listed along with error function values in Table 5 and all the pollutant uptake values calculated using two-parameter models are plotted in Fig. 7a.

3.2.3.1. Langmuir adsorption isotherm model

The Langmuir isotherm showed comparably fair results. The separation factor R_L is the parameter that states the adsorption behavior in the case of Langmuir isotherm. The R_L value was found to be 0.05, which shows favorable

Table 2
Two-parameter adsorption isotherm model

Model	Non-linear form	Parameters
Langmuir	$q_e = \frac{q_L k_L C_e}{1+k_L C_e}$ $R_L = \frac{1}{1+k_L C_0}$	k_L (L/mg) q_L(mg/g) R_L
Freundlich	$q_e = k_F C_e^{1/n_F}$	n_F (g/L) k_F(L/g)
BET	$q_e = \frac{B_{BET} C_e q_{BET}}{(C_0 - C_e)\left(1+(B_{BET}-1)\frac{C_e}{C_0}\right)}$	B_{BET} q_{BET}
Flory Huggins	$\frac{\theta}{C_0} = k_{FH}(1-\theta)^{n_{FH}}$; $\theta = 1-\frac{C_e}{C_0}$	n_{FH} k_{FH}

Table 3
Three-parameter adsorption isotherm model parameters

Model	Non-linear form	Parameters
Redlich–Peterson	$q_e = \frac{k_{RP} C_e}{1+a_{RP} C_e^{b_{RP}}}$	k_{RP} (L/mg) a_{RP} (L/mg) b_{RP}
Langmuir–Freundlich	$q_e = \frac{k_{LF} C_e^{c_{LF}}}{\left(1+a_{LF} C_e^{c_{LF}}\right)}$	k_{LF} a_{LF} c_{LF}
Toth	$q_e = \frac{q_{TOTH} C_e}{\left(b_{TOTH} + C_e^{n_{TOTH}}\right)^{(-1/n_{TOTH})}}$	q_{TOTH} (mg/g) b_{TOTH} n_{TOTH}

Table 4
Error functions

Sum of the absolute errors (EABS)	$\sum_{n=1}^{N} \left\| q_{e,\exp} - q_{e,\mathrm{iso}} \right\|_{ni}$
Average relative error (ARE)	$\frac{100}{n} \sum_{n=1}^{n} \left\| \frac{q_{e,\exp} - q_{e,\mathrm{iso}}}{q_{e,\mathrm{iso}}} \right\|_n$
Chi-square test (χ^2)	$\sum_{i=1}^{n} \left\| \frac{q_{e,\exp} - q_{e,\mathrm{iso}}}{q_{e,\mathrm{iso}}} \right\|$

isotherms. For R_L = 1, it is linear, R_L < 0, it is irreversible and R_L > 1, it is unfavorable. The isotherm gave a fair linear correlation coefficient (R^2 = 0.794). It generally works on two assumptions, the first being, monolayer occupancy of the surface of the adsorbent by the pollutant and the second being, the surface is completely uniform and energetically homogeneous. A low value (<1) of k_L of 0.01093 hints the high affinity of pollutants with the adsorbent. q_L value for the Langmuir model was found to be 283 mg/g, which is fairly high and points high pollutant uptake by SSP. Also, a low value of the error function shows the similarity between the experimental and model values [21].

3.2.3.2. Freundlich adsorption isotherm model

Freundlich model showed the best result with high R^2 (0.9437) and n_F value came 3.197, which is between 1 and 10 and it is favorable. The Freundlich isotherm parameter $1/n_F$ measures the adsorption intensity of pollutant ions on adsorbent and Freundlich constant k_F is adsorption capacity. The value of $1/n_F$ was found to be 0.3131 for different concentrations, which shows that mainly the physical process controls the adsorption. These values also revealed greater heterogeneity of the adsorbent sites [22]. The values of ARE, EABS, and χ^2 are 0.4473, 1, and 0.8735, respectively, which shows that Freundlich isotherm gives a favorable plot for the present study. Preferentially, stronger binding sites are occupied early and the binding strength decreases after that. It is originally empirical but was later interpreted as sorption to hetero surface or surface supporting sites of varied affinities [23].

3.2.3.3. BET adsorption isotherm model

The BET model assumes that several layers of adsorbate molecules are formed at the surface of the sorbent and the Langmuir equation applies to each layer. A further assumption of the BET model is that a given layer need not complete formation before initiation of subsequent layers; the equilibrium condition will, therefore, involve several types of surfaces, in the sense of some layers of molecules on each surface. BET is a constant which indicates the energy of interaction between the solute and the adsorbent surface, q_{BET} is an amount of solute adsorbed forming a complete monolayer (mg/g), which is 233 (Table 5) [24].

3.2.3.4. Flory Huggins adsorption isotherm model

The Flory Huggins model also showed satisfactory results in the study. It generally indicates the degree of surface coverage. K_{FH} is the equilibrium constant and n_{FH} is the number of ions of the pollutant occupying the sites of the adsorbent. A higher value (>1) of "n_{FH}" shows a greater amount of pollutants being occupied onto the adsorbent. The n_{FH} value obtained was 2.71 reasonably high shows a favorable plot for the present study [21].

3.2.4. Three parameter models

Three parameter models were also found to evaluate the performance of the experiments. Three types of three-parameter models were used for the present study and their model parameters are listed in Table 6 and the plots are given in Fig. 7b.

3.2.4.1. Redlich–Peterson adsorption isotherm model

Redlich–Peterson model is a hybrid three-parameter isotherm, which combined the parameter of both Langmuir and Freundlich isotherms. It can be used for both homogeneous and heterogeneous systems. If the exponent

Table 5
Two-parameter adsorption isotherm model parameters and error function values

Model	Parameters	SSP	Inference (Vishali and Mullai [21])
Langmuir	k_L (L/mg)	0.01093	<1 high affinity
	q_L (mg/g)	283	High adsorption capacity
	R_L	0.05	$0 < R_L < 1$ favorable
	EABS	6	
	ARE	2.1521	
	χ^2	13	
	R^2	0.794	
Freundlich	n_F (g/L)	3.1974	1–10 favorable
	k_F (L/g)	35.113	>1 higher affinity and heterogenity
	EABS	1	
	ARE	0.4473	
	χ^2	0.8735	
	R^2	0.9437	
BET	B_{BET} (mg/L)	19	High adsorption capacity
	q_{BET} (mg/g)	233	
	EABS	2	
	ARE	0.8735	
	χ^2	13	
	R^2	0.8594	
Flory Huggins	n_{FH}	2.71	$n > 1$, greater number of pollutants occupying the binding sites
	k_{FH}	0.0856	

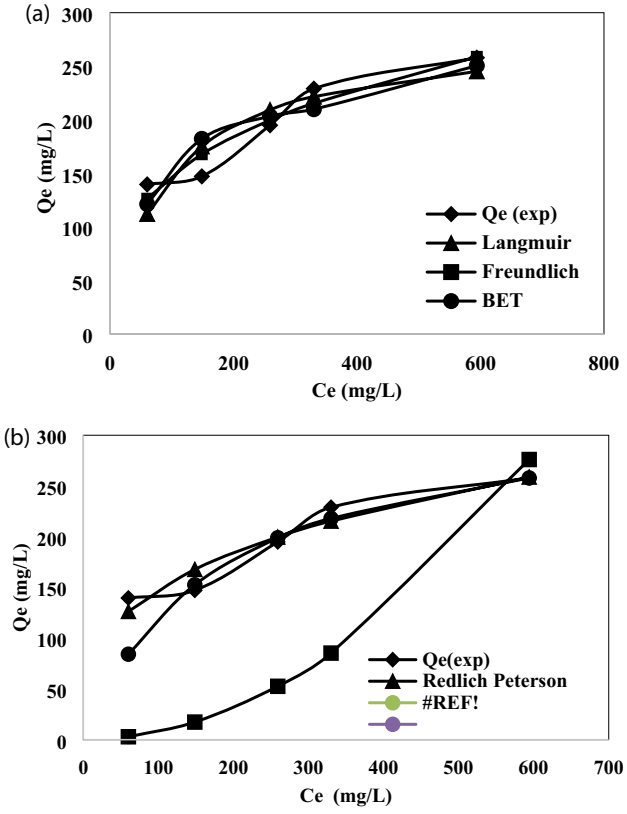

Fig. 7. (a) Two-parameter and (b) three-parameter adsorption isotherm models for SSP.

component b_{RP} lies between 0 and 1, then the model supported the heterogeneous system of sorption (Table 6). The b_{RP} value is 0.687 and it confirms the heterogeneous nature [25]. Higher values of k_{RP} (6,116 L/mg), and R^2 (0.9437) and lower values of error functions confirmed the suitability of this model.

3.2.4.2. Langmuir–Freundlich adsorption isotherm model

The Langmuir–Freundlich isotherm is another three-parameter model which represents the limiting behavior of the equation. The characteristic of the isotherm is that at low concentrations of sorbate, the isotherm reduces to Freundlich isotherm and does not obey Henry's law. When the concentrations of the sorbate are high, it represents monolayer formation [26]. The values of all the three error functions were considerably found to be small relative to the other values. The value of EABS, ARE, and χ^2 was found to be 57, 13.12, 23, respectively and the k_{LF} was also found to be well within the range.

3.2.4.3. Toth adsorption isotherm model

Toth isotherm model was used in the present study to throw light on the heterogeneous sorption systems in play. It could be successfully applied to both low and high concentration of adsorbates. The model's constant values revealed the heterogeneity of the adsorbent surface [25]. It is derived empirically to enhance the fitness of the model with experimental data. Though Toth model showed large deviations from the experimental data, it was relatively

Table 6
Three-parameter adsorption isotherm model parameters and error function values

Model	Parameters	SSP	Inference (Vishali and Mullai [21])
Redlich–Peterson	k_{RP} (L/mg)	6,116	
	a_{RP} (L/mg)	174	$0 < b_{RP} < 1$ supports heterogeneous system of adsorption
	b_{RP}	0.687	
	EABS	1	
	ARE	0.425	
	χ^2	5	
	R^2	0.9437	
Langmuir–Freundlich	k_{LF}	1.800	
	a_{LF}	5.407×10^{-3}	Non-occurrence of chemisorptions
	c_{LF}	1.01	
	EABS	57	
	ARE	13.12	
	χ^2	23	
	R^2	0.8636	
Toth	q_{TOTH} (mg/g)	7.813×10^{-4}	
	b_{TOTH}	0.9981	
	n_{TOTH}	1.014	>1 indicates heterogeneity
	EABS	535	
	ARE	1,196	
	χ^2	444	
	R^2	0.9048	

more in agreement with the experimental data compared to the other models tried. Though the correlation coefficient (R^2) value was close to 1(0.9048), the error functions EABS, ARE, and χ^2 showed large values. It indicates that the Toth model does not fully correlate with the experimental data.

3.3. Modeling of coagulation kinetics

The role of equilibrium time plays a vital part in the wastewater treatment. The maximum uptake of pollutants by the coagulant was utilized to find the kinetic model parameters. For the kinetic modeling, both the simulated paint factory effluent (SPFE) and the real paint factory effluent (RPFE) were considered by utilizing shrimp shell powder (SSP) and chitosan as a coagulant. Different kinetic models were therefore tried and tested during the course. Selection of the most suitable model was based on (a) comparison of the experimental and simulated data, and (b) evaluation of the correlation between coagulation properties and model theory [27].

The following models were investigated, that is; first-order, second-order, Elovich, Bhangham, intraparticle

Table 7
Linear form of kinetic models

Models	Linear equation
First-order kinetic model	$\ln(C_0/C) = k_1 t$
Second-order kinetic model	$(1/C) = k_2 t + (1/C_0)$
Elovich	$q_t = \frac{1}{\beta_E}\ln\left(\propto_E \beta_E\right) + \frac{1}{\beta_E}\ln t$
Bangham model	$\log q_t = \log k_B + \frac{1}{m_B}\log t$
Intraparticle diffusion model	$q_t = k_{id} t^{0.5} + I$
Avrami model	$\ln\left(-\ln\left(1-\frac{q_t}{q_e}\right)\right) = \ln\left(k_{Av}\right) + m_{Av}\ln t$

diffusion, and Avrami. Excel spreadsheets were used to find the equilibrium uptake of pollutants from the experiment ($q_{e,\exp}$) and kinetic model ($q_{e,\text{cal}}$). Confirmations were made when the (R^2) values were much higher. The linear form of kinetic models is consolidated in Table 7 [28].

3.3.1. First-order and second-order kinetic model

During the settling span, the residual turbidity was declined with raise in time. It is due to the non-availability of a number of the particles in due course of time. Generally, the residual turbidity was measured in NTU, but it could be converted into concentration term with the unit of mg/L, by multiplying with 2.3 [29].

The plots were made between time and $\ln(C_0/C)$ (Fig. 8), the model parameters were tabulated in Tables 8a and b. The plots are linear with $R^2 > 0.9$, but do not pass through the origin. In addition to this, the existence of a negative intercept also indicated that this system is in disagreement with the first-order kinetic model.

The linear form of the second-order equation is plotted in Fig. 9. By matching the experimental and graphical $1/C_0$ (mg/L) (Tables 8a and c), it was concluded that the second-order model favors the system [30].

3.3.2. Elovich kinetic model

The Elovich kinetic model, which fundamentally supports chemisorption, was evaluated by predicting the slope and intercept of the linear plot between t vs. q_t (Fig. 10). The heterogeneity nature of the coagulant surface and the absence of chemisorptions was affirmed by the higher values of α_E (>1) and the smaller values of β_E (<1), respectively [24].

3.3.3. Intra particle diffusion kinetic model

The intraparticle diffusion rate constant k_{id} values are found from the slopes of q_t vs. $t^{0.5}$ plots (Fig. 11). The correlation coefficient ($R^2 > 0.9$) was in good agreement with the model parameters (Table 9). A line that flops to move through the origin would express some degree of film diffusion control. The model values are supported that besides to intraparticle diffusion, film diffusion was also answerable for impacting the adsorption [31].

3.3.4. Bangham model

The Bangham model parameters (Table 9) were estimated from the basic plot between log$t$ vs. logq_t (Fig. 12). The suitability of the coagulant for the treatment of SPFE was affirmed by the larger values of k_B (>1). $R^2 > 0.9$ pointed the linearity of the values [24].

3.3.5. Avrami model

The Avrami model was plotted in Fig. 13, which was used to evaluate the model parameters k_{Av} and m_{Av}. The impact of contact time on the treatment process and to find the surface area of the coagulant model parameters was utilized. The adsorption process is limited either by surface reaction

Table 8a
Kinetic model parameters

Parameter	First-order kinetic model	Second-order kinetic model
$t_{0.5}$ (min)	$0.6931/k_1$	$0.6931/k_2$
β (m^3/kg s)	$2k_1$	$2k_2$
D (kg^2/m s)	$k_B T/\beta$	$k_B T/\beta$
K_{Rc} (1/min)	$4\,k_B T/3\,\mu$	$4\,k_B T/3\,\mu$
E	k_1/K_{Rc}	k_2/K_{Rc}

Table 8b
Model parameters of first-order kinetic model

	SSP		
First-order	SPFE	RPFE	Chitosan
R^2	0.9887	0.9965	0.8851
k_1 (1/min)	0.0123	0.0194	0.0065
$t_{0.5}$ (min)	56.34	35.72	106.63
β (m^3/kg s)	0.0246	0.0279	0.013
D (kg^2/m s)	0.169×10^{-20}	0.149×10^{-20}	0.321×10^{-20}
K_{Rc} (1/min)	3.87×10^{-19}	3.71×10^{-19}	3.87×10^{-19}
E	3.178×10^{16}	5.22×10^{16}	3.178×10^{16}

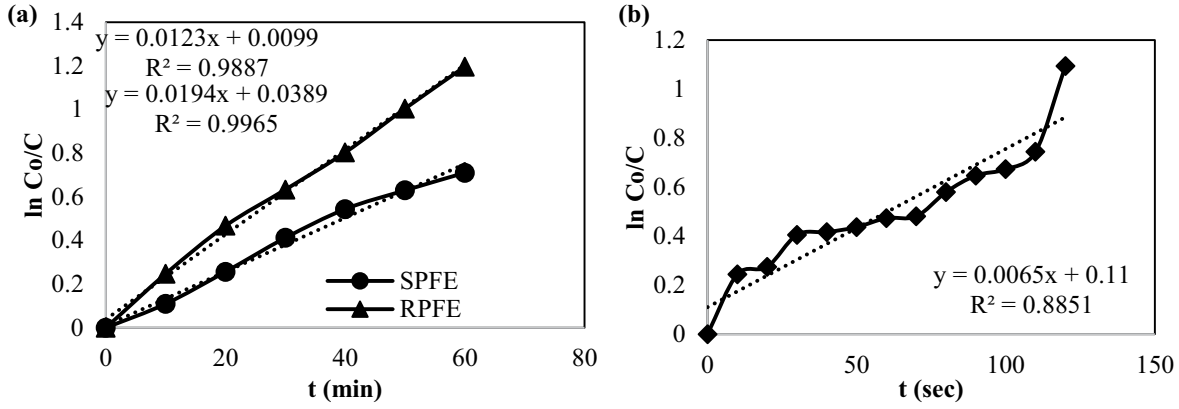

Fig. 8. Kinetic plots of first-order kinetic model (a) SSP and (b) chitosan.

($m_{Av} > 1$) or not is feasibly found out using this model parameter (Table 9) [32].

3.4. Cluster size distribution

The growth of flocs was found as a function of time, which serves as a precursor to find the cluster size distribution. Using Eq. (4) for the monomers ($m = 1$), dimmers ($m = 2$), and trimmers ($m = 3$), the values were predicted.

$$N_m(t) = 4N_0^m (kt)^{m-1} (2 + kN_0 t)^{-(m+1)} \quad (4)$$

From Fig. 14, it is noticed that the nature of the lines was identical for all the three cases viz., (i) SPFE vs. SSP, (ii) RPFE vs. SSP, and (iii) SPFE vs. chitosan. The rapid drop of monomer particles was happened compared to the decline in the total number of particles. Once all the monomer particles are entirely dropped, it makes the driving force for the settling of dimmer and trimmer particles [29–31].

Table 8c
Model parameters of second-order kinetic model

	SSP		
Second-order	SPFE	RPFE	Chitosan
R^2	0.9346	0.9787	0.8033
k_2 (L/mg min)	9×10^{-7}	800×10^{-7}	7×10^{-7}
$t_{0.5}$ (min)	111.11	23.75	0.01
β (m^3/kg s)	0.018	0.00016	0.014
D (kg^2/m s)	2.323×10^{-19}	0.026×10^{-19}	2.98×10^{-19}
K_{Rc} (1/min)	3.98×10^{-18}	3.71×10^{-18}	3.98×10^{-18}
E	2.26×10^{11}	215.6×10^{11}	1.75×10^{11}
Graph ($1/C_0$)	1×10^{-4}	19×10^{-4}	7×10^{-5}
Experiment ($1/C_0$)	1.2×10^{-5}	21.9×10^{-4}	6.35×10^{-5}

3.5. Determination of thickener area

To determine the area of the clarifier–thickener, settling data obtained from batch tests were used. To concentrate the sludge from SPFE with an initial concentration ranged from 1,200 to 2,700 mg/L and at the rate of 1,000 L/d, the Kynch theory was used. From the batch settling data, few points were selected and the corresponding time and sludge bed height were named as (min), Z_L (m), respectively. The tangent was drawn for the selected points and the meeting point of the tangent line on the Y-axis, that is, sludge bed height, was

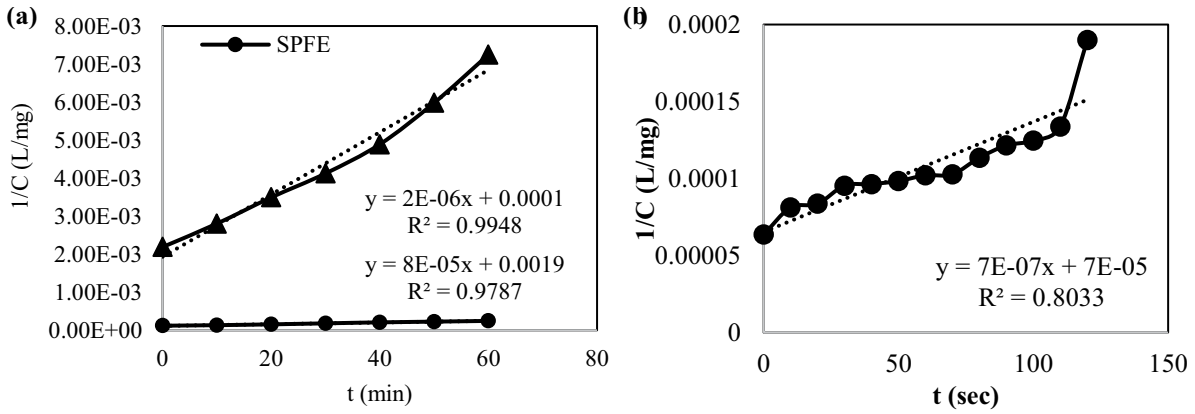

Fig. 9. Kinetic plots of second-order kinetic model (a) SSP and (b) chitosan.

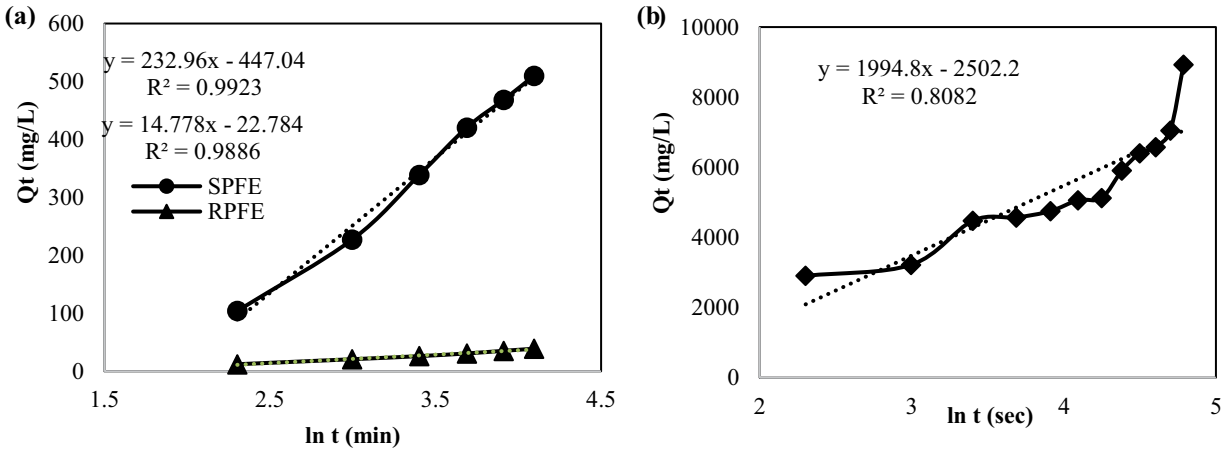

Fig. 10. Kinetic plots of Elovich kinetic model (a) SSP and (b) chitosan.

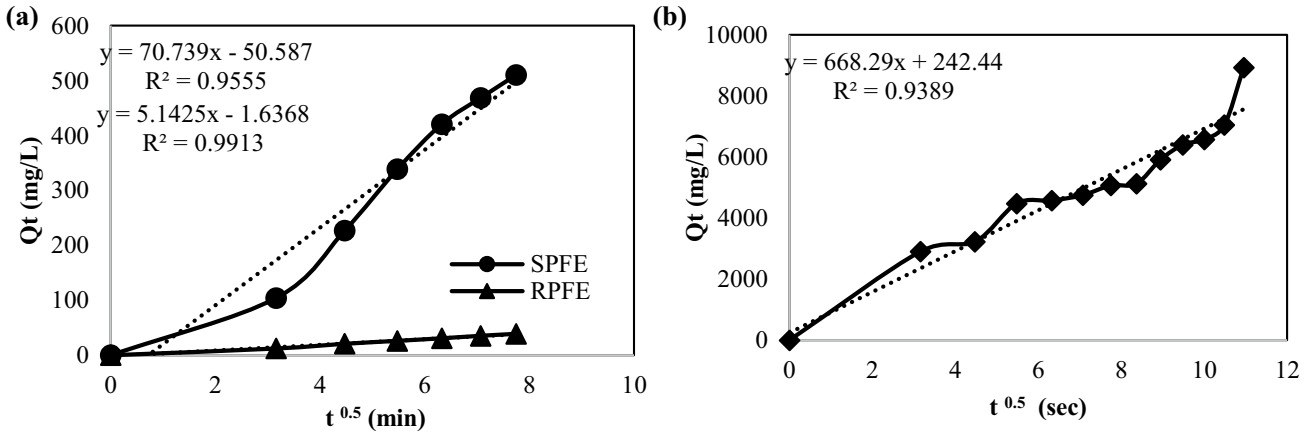

Fig. 11. Kinetic plots of intraparticle diffusion kinetic model (a) SSP and (b) chitosan.

Table 9
Kinetic model parameter values

Kinetic model parameters		SSP		
		SPFE	RPFE	Chitosan
Elovich	R^2	0.9923	0.9886	0.8082
	α_E	34.20	23.01	34142
	β_E	4.29×10^{-3}	0.067	5.013×10^{-4}
Intra particle diffusion	R^2	0.955	0.9913	0.9389
	k_{id}	70.739	5.142	40,097
	I	–50.59	–1.637	242.4
Bhangam	R^2	0.9779	0.9943	0.915
	m_B	1.11	1.56	2.480
	k_B	14.51	2.919	3,920
Avrami	R^2	0.9982	0.987	0.987
	m_{Av}	1.487	1.102	1.53
	$k_{Av} \times 10^{-3}$	7.17	28.56	3.58

marked as Z_i (m). Based on these three data, that is, (min), Z_L (m), Z_i (m), the sludge concentration (C_L), underflow sludge concentration (C_U), and settling velocity (V_L) were calculated using following formulae (Eqs. (5)–(8)) [33]. The plot (Fig. 15a) was made between $\frac{V_L}{\left(\frac{1}{C_L}-\frac{1}{C_U}\right)}$ vs. C_L to determine the maximum required clarifier–thickener area. At the optimized conditions to treat 1,000 L/d flow of SPFE with the initial concentration ranged between 1,200 and 2,700 mg/L the clarifier–thickener area required was varied from 0.0074 to 0.0110 m². It was noticed that with an increase in the initial concentration of effluent, the requirement of the clarifier–thickener area was also raised (Fig. 15b) [34].

$$\text{Slurry concentration, } C_L = \frac{C_0 Z_0}{Z_i},\ \text{kg/m}^3 \quad (5)$$

$$\text{Underflow concentration, } C_U = \frac{C_0 Z_0}{Z_U},\ \text{kg/m}^3 \quad (6)$$

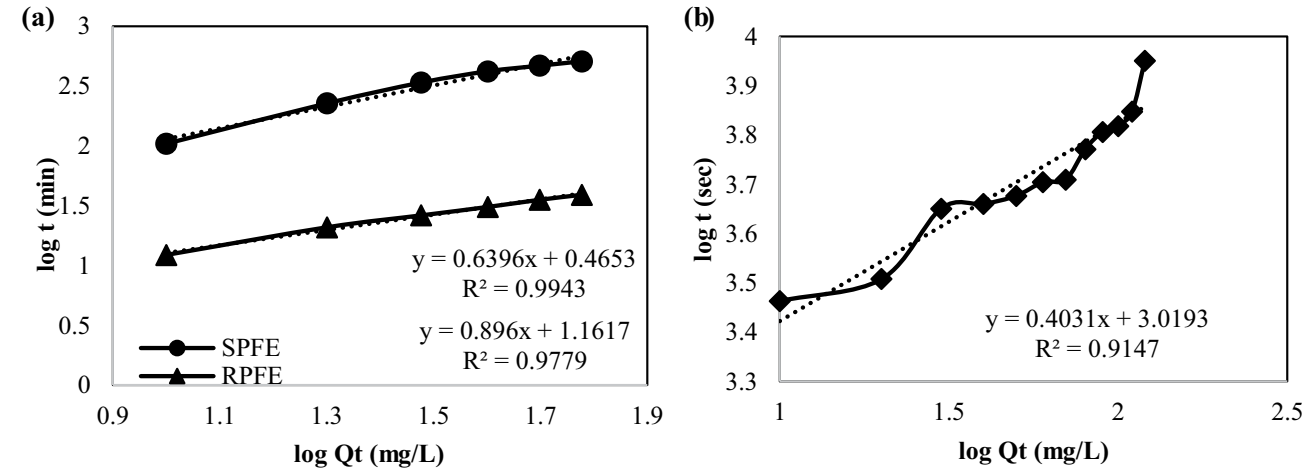

Fig. 12. Kinetic plots of Bhangham kinetic model (a) SSP and (b) chitosan.

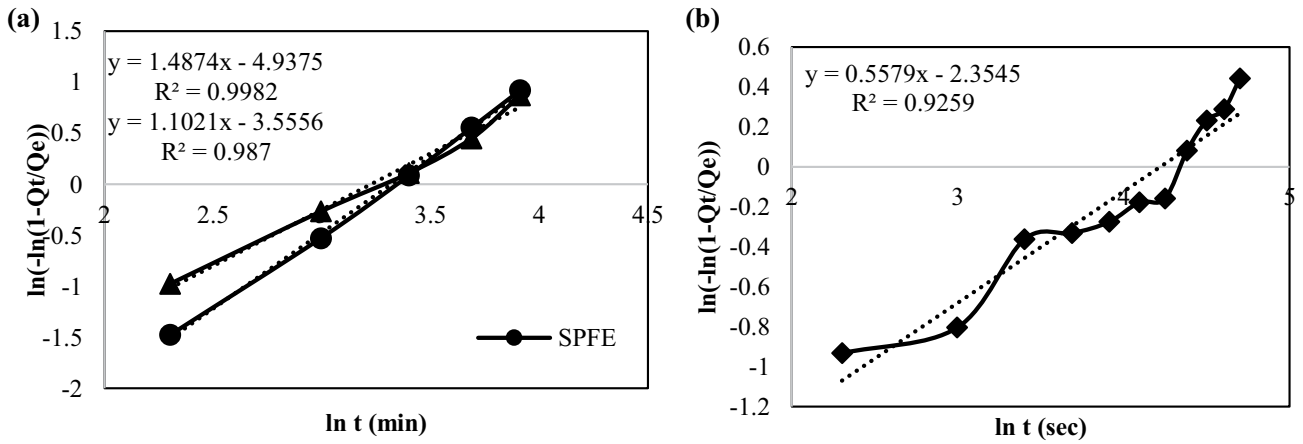

Fig. 13. Kinetic plots of Avrami kinetic model (a) SSP and (b) chitosan.

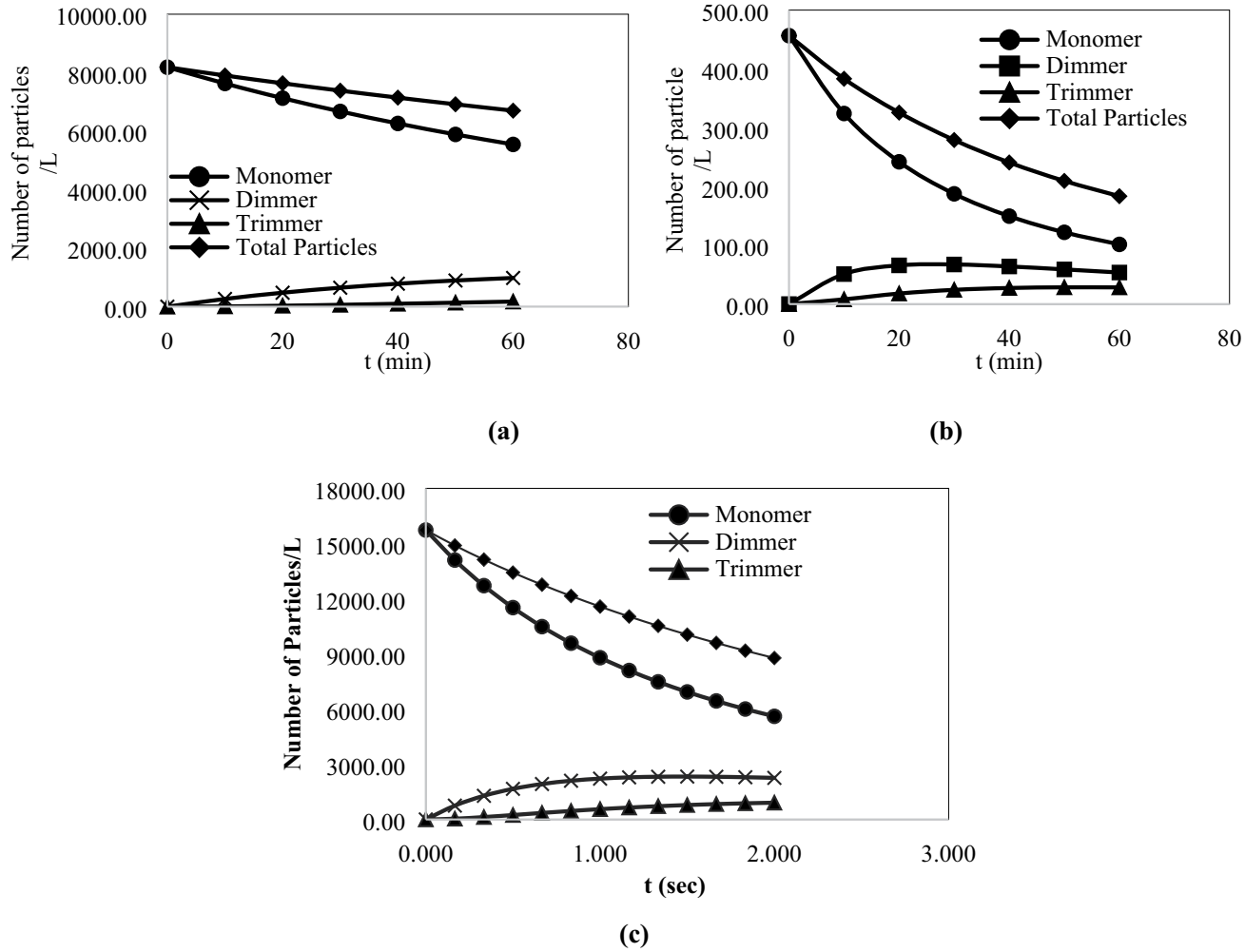

Fig. 14. (a) SPFE vs. SSP, (b) RPFE vs. SSP, and (c) SPFE vs. chitosan.

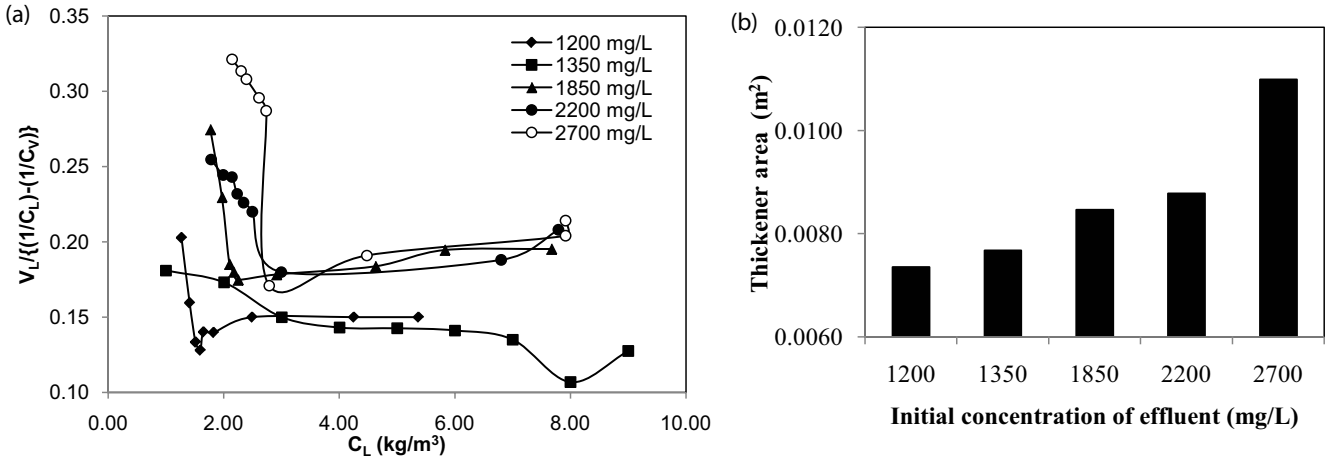

Fig. 15. Thickener area (a) calculation for different and (b) requirement as a function of initial concentration of effluent.

$$\text{Settling velocity, } V_L = \frac{Z_i - Z_L}{\theta_L}, \text{ m/s} \quad (7)$$

$$\text{Thickener area, } A = \frac{FC_0}{\frac{V_L}{\left(\frac{1}{C_L} - \frac{1}{C_U}\right)}}, \text{ m}^2 \quad (8)$$

where F is the rate of feed, m³/s; C_0 is the initial concentration, kg/m³; C_U is the under flow concentration, kg/m³; Z_0 is the initial sludge bed height, m; Z_U is the final sludge bed height, m; V_L is the settling velocity, m/s.

4. Conclusions

The present work brings the first example for explaining the performance of SSP and chitosan as a coagulant on the treatment of SPFE and their isotherm mechanisms, kinetic mechanisms, thickener design. Based on the observed results, the following conclusions were derived.

- 200 rpm (for 5 min) of rapid mixing, 80 rpm (20 min) of sow mixing, and 40 min of settling span resulted in maximum removal efficiency of 93% (color) and 82% (turbidity).
- Velocity gradient and the Camp number are found to be the function of mixing speed, which gave the maximum results at the optimum value of 562 1/s and 8.05, respectively.
- The adsorption isotherm studies were performed at the optimum conditions, which showcased that the process belongs to physisorption and the heterogeneity nature of the coagulant.
- From the kinetics studies, it was understood that the similarity between the experimental and model parameters confirms the second-order kinetic system. The results of the intraparticle diffusion model indicated that the film diffusion influenced the process in addition to the intraparticle diffusion.
- Based on the Kynch theory approach for the flow rate of 1,000 L/d of SPFE, the thickener area was determined. The required area was ranged between 0.0074 and 0.011 m² for the initial concentration of 1,200–2,700 mg/L, respectively.

Symbols and abbreviations

a_{LF} — Model constant of Langmuir–Freundlich model
a_{RP} — Redlich–Peterson model constant, L/mg
B_{BET} — Constant of BET model
b_K — Khan model constant
b_{RP} — Redlich–Peterson model exponent
b_{TOTH} — Toth model constant
C_0, C_e, C_t — A concentration of the solute, at t = 0, at equilibrium and time "t" in the effluent, mg/L
c_{LF} — Model constant of Langmuir–Freundlich model
D — Brownian diffusion coefficient, kg²/m s
D_i — Effective diffusivity, cm²/min
E_f — Mean free energy of adsorption per molecule of adsorbate, kJ/mol
E — Collision efficiency, dimensionless
I — A thickness of the boundary layer, mg/g
k_{FH} — Uptake of pollutants in Florry Huggins model
k_{LF} — The sorption capacity of the Langmuir–Freundlich model
k_{Av} — Kinetic constant in the model Avrami model
k_B — Kinetic constant in the model Bangham model, mg/g min
k_{id} — Kinetic rate constant in the intraparticle diffusion model, mg/g min$^{0.5}$
k_F — Adsorption capacity from Freundlich model, L/g
k_L — Langmuir adsorption constant, L/mg
k_{RP} — Redlich–Peterson model isotherm constant, L/mg
k_{Bo} — 1.381 × 10^{-23} Boltzmaan constant, m² kg/ s² K
K_{Rc} — Smoluchowski rate constant for rapid coagulation, 1/min
m — Total mass of adsorbent, g
m_{Av} — Avrami model parameter

m_B — Bangham model parameter
n — Number of measurements, isotherms
n — Order of the coagulation process
n_F — Adsorption intensity from Freundlich model, g/L
n_{FH} — Number of pollutants occupying the binding sites in Florry Huggins model
n_{TOTH} — Toth model exponent
N_0 — Initial particle concentration, mg/L
p — Number of parameters present in the adsorption isotherm model
q_t, q_e — Total quantity of pollutant adsorbed at time "t" and equilibrium, mg/g
$q_{e,exp}$, $q_{e,iso}$ — Equilibrium uptake of pollutants from the experiment & isotherm model, mg/g
q_L — Monolayer adsorption capacity from Langmuir model, mg/g
q_{TOTH} — Adsorption capacity from Toth model, mg/g
q_{BET} — Amount of pollutant adsorbed (mg/g) in the BET model
R — Gas constant, 8.314 J/mol K
R^2 — Correlation coefficient
R_L — Separation factor
T — Absolute temperature, K
t — Coagulation process time, min
$t_{0.5}$ — Time required for 50% removal of initial concentration, min
α_E — Initial adsorption rate in the Elovich model, mg/mg
β — Friction factor due to shear stress, m^3/(kg s)
β_E — Desorption constant in the Elovich model, g/mg
ε — Polanyi potential
μ — Effluent viscosity, kg m/sec

References

[1] S. Vishali, P. Rashmi, R. Karthikeyan, Evaluation of wasted biomaterial, crab shells (*Portunus sanguinolentus*), as a coagulant, in paint effluent treatment, Desal. Water Treat., 57 (2016) 13157–13165.
[2] H.A. Coruh, Use of Calcium Alginate as a Coagulant in Water Treatment, Dissertation School of Natural and Applied Sciences of Middle East Technical University, Middle East, 2007.
[3] Available at: http://www.iwawaterwiki.org/xwiki/bin/view/Articles/CoagulationandFlocculationinWaterandWastewaterTreatment
[4] K. Loganathan, J. Saththasivam, S. Sarp, Removal of microalgae from seawater using chitosan-alum/ferric chloride dual coagulations, Desalination, 433 (2018) 25–32.
[5] C.-Y. Yin, Emerging usage of plant-based coagulants for water and wastewater treatment, Process Biochem., 45 (2010) 1437–1444.
[6] E. Hart, Optimizing Coagulant Conditions for the Worcester Water Filtration Plant, Dissertation, Worcester Polytechnic Institute, Massachusetts, 2001.
[7] Available at: http://ocw.tudelft.nl/fileadmin/ocw/courses/DrinkingWaterTreatment1
[8] R.M. Shamsuddin, C.J.R. Verbeeka, M.C. Laya, Settling of bentonite particles in gelatin solutions for stickwater treatment, Procedia Eng., 148 (2016) 194–200.
[9] Y. Oua, R. Lia, R. Lianga, Experimental study on the impact of NaCl concentration on the flocculating settling of fine sediment in static water, Procedia Eng., 154 (2016) 529–535.
[10] R. Hosny, M. Fathy, M. Ramzi, T.A. Moghny, S.E.M. Desouky, S.A. Shama, Treatment of the oily produced water (OPW) using coagulant mixtures, Egypt. J. Pet., 25 (2016) 391–396.
[11] M.A. Rahman, M.M. Hossain, A. Samad, A.M.S. Alam, Removal of arsenic from ground water with shrimp shell, Dhaka Univ. J. Sci., 60 (2012) 175–180.
[12] F. Massimiliano, P. Ludovico, Use of non-treated shrimp-shells for textile dye removal from wastewater, J. Environ. Chem. Eng., 4 (2016) 4100–4106.
[13] T. Kinoshita, K. Nakaishi, Y. Kuroda, Determination of kaolinite floc size and structure using interface settling velocity, Appl. Clay Sci., 148 (2017) 11–16.
[14] APHA, Standard Methods for the Examination of Waste and Wastewater, 16th ed., American Public Health Associations, New York, NY, 1995.
[15] S. Vishali, S. Picasso, M. Rajdeep, R. Nihal, Shrimp shell waste – a sustainable surrogate solution for chemical coagulants in industrial effluent treatment, Desal. Water Treat., 104 (2018) 111–120.
[16] J.M. Thamer, E. Shakir, Effect of settling time, velocity gradient and Camp number on turbidity removal for oilfield produced water, Egypt. J. Pet., 27 (2017) 31–36.
[17] F.H. Chi, W.P. Cheng, Use of chitosan as coagulant to treat wastewater from milk processing plant, J. Polym. Environ., 14 (2006) 411–417.
[18] D. Branes, P. Bliss, B. Gould, Water and Wastewater Engineering System, Pitman Publishing Limited, London, 1984.
[19] G. Tchobanoglous, Wastewater Engineering Treatment and Reuse, 4th ed., Mc Graw-Hill, New York, NY, 2003.
[20] K. Vijayaraghavan, T.V.N. Padmesh, K. Palanivelu, M. Velan, Biosorption of nickel(II) ions onto *Sargas sumwightii*: application of two-parameter and three-parameter isotherm models, J. Hazard. Mater., 133 (2006) 304–308.
[21] S. Vishali, P. Mullai, Analysis of two-parameter and three-parameter isotherms by nonlinear regression for the treatment of textile effluent using immobilized *Trametes versicolor*: comparison of various error functions, Desal. Water Treat., 57 (2016) 27061–27072.
[22] J.P. Kushwaha, V.C. Srivastava, D.D. Mall, Treatment of dairy wastewater by commercial activated carbon and bagasse fly ash: parametric, kinetic and equilibrium modelling, disposal studies, Bioresour. Technol., 101 (2010) 3474–3478.
[23] M. Akhtar, S. Iqbal, M.I. Bhanger, M. Zia-Ul-Haq, M. Moazzam, Sorption of organo phosphorous pesticides onto chickpea husk from aqueous solutions, Colloids Surf., B, 69 (2009) 63–70.
[24] R. Nadeem, M.H. Nasir, M.S. Hanif, Pb(II) sorption by acidically modified *Cicerarientinum* biomass, Chem. Eng. J., 150 (2009) 40–48.
[25] M.A. Hossain, H.H. Ngo, W.S. Guo, T.V. Nguyen, Palm oil fruit shells as biosorbent for copper removal from water and wastewater: experiments and sorption models, Bioresour. Technol., 113 (2012) 97–101.
[26] Y.S. Ho, J.F. Porter, G. Mckay, Equilibrium isotherm studies for the sorption of methylene blue onto peat: copper, nickel and lead single component systems, Water Air Soil Pollut., 141 (2002) 1–33.
[27] E. Repo, Edta- and Dtpa-Functionalized Silica Gel and Chitosan Adsorbents for the Removal of Heavy Metals from Aqueous Solutions, Dissertation Lappeenranta University of technology, Finland, 2011.
[28] A. Rathinam, B. Maharshi, S.K. Janardhanan, R.R. Jonnalagadda, B.U. Nair, Biosorption of cadmium metal ion from simulated wastewaters using *Hypnea valentiae* biomass: a kinetic and thermodynamic study, Bioresour. Technol., 101 (2010) 1466–1470.
[29] M. Magesh kumar, R. Karthikeyan, Modeling the kinetics of coagulation process for tannery industry effluent treatment using *Moringa oleifera* seeds protein, Desal. Water Treat., 57 (2016) 14954–14964.
[30] A. Sari, D. Mendil, M. Tuzen, M. Soylak, Biosorption of Cd(II) and Cr(III) from aqueous solution by moss (*Hylocomium splendens*) biomass: equilibrium, kinetic and thermodynamic studies, Chem. Eng. J., 144 (2008) 1–9.
[31] S. Vishali, R. Karthikeyan, Application of green coagulants on paint industry effluent – a coagulation-flocculation kinetic study, Desal. Water Treat., 122 (2018) 112–123.

[32] R. George, S. Sugunan, Kinetics of adsorption of lipase onto different mesoporous materials: evaluation of Avrami model and leaching studies, J. Mol. Catal. B: Enzym., 105 (2014) 26–32.
[33] C.A. Fernando, Solid Liquid Separation in the Mining Industry, Springer International Publishing, Swizterland, 2014.
[34] M. Magesh Kumar, R. Karthikeyan, K. Anbalagan, M. Nishant Bhanushali, Coagulation process for tannery industry effluent treatment using *Moringa oleifera* seeds protein: kinetic study, pH effect on floc characteristics and design of a thickener unit, Sep. Sci. Technol., 51 (2016) 2028–2037.